Experimental Studies of Overmoded Relativistic Backward-Wave Oscillators

David K. Abe, *Member, IEEE*, Yuval Carmel, *Senior Member, IEEE*, Susanne M. Miller, *Member, IEEE*, Alan Bromborsky, Baruch Levush, *Senior Member, IEEE*, Thomas M. Antonsen, Jr., *Member, IEEE*, and William W. Destler, *Fellow, IEEE*

***Abstract*—Internal field-emission breakdown in the electrodynamic structures of high-power microwave (HPM) devices can seriously limit the device's output power and pulse duration. Increasing the diameter of the electrodynamic structure to several times an electromagnetic wavelength can reduce these internal fields to below critical breakdown levels, but may introduce mode competition as an unwanted side effect. This paper presents the design and results of experiments with overmoded $(D/\lambda \sim 3)$, sinusoidally corrugated backward-wave oscillators (BWO's) that successfully produced TM$_{01}^{\odot}$, high-power microwave radiation in the frequency range of 5.2–5.7 GHz. Overmoded BWO's reproducibly generated ~200 MW of peak power with corresponding efficiencies of ~4%. Pulse shortening was not observed in any of the experiments. The radiation generated by the devices was highly coherent (typically, $\Delta f/f < 0.5\%$) and corresponded to a fundamental TM$_{01}^{\odot}$-mode interaction. The experimental results were compared with calculations made with recently developed nonlinear models; the measured data are shown to agree favorably with theory. The results of the experiments and modeling demonstrate that overmoded electrodynamic structures can be used to decrease internal electric field stresses while avoiding multimode generation and maintaining good spectral purity.**

***Index Terms*— Backward-wave oscillator (BWO), high-power microwave (HPM), overmoded.**

I. Introduction

APPLICATIONS exist for single-shot high-power microwave (HPM) devices capable of generating ≥ 1 GW of output power at centimeter wavelengths. These applications include directed-energy warfare and laboratory sources for the vulnerability and susceptibility testing of electronic systems. However, as the output power increases, a decrease in the temporal duration of the microwave pulse has been observed in many linear beam HPM devices [1], [2]. This pulse shortening has been attributed to plasma-related phenomena and to internal breakdown caused by field emission from conducting surfaces and is a serious limiting factor in high-power applications.

Manuscript received August 29, 1997; revised January 16, 1998. This paper was presented in part at the International Workshop on High Power Microwave Generation and Pulse Shortening, Edinburgh, U.K., June 1997. This work was supported by the U.S. Army Research Laboratory and, in part, by the U.S. Air Force Office of Scientific Research (HPM MURI program).

D. K. Abe and B. Levush are with the U.S. Naval Research Laboratory, Washington, DC 20375 USA.

Y. Carmel, T. M. Antonsen, Jr., and W. W. Destler are with the Institute for Plasma Research, University of Maryland, College Park, MD 20742 USA.

S. M. Miller is with ENSCO, Springfield, VA 22150 USA.

A. Bromborsky is with the U.S. Army Research Laboratory, Adelphi, MD 20783 USA.

Publisher Item Identifier S 0093-3813(98)04291-X.

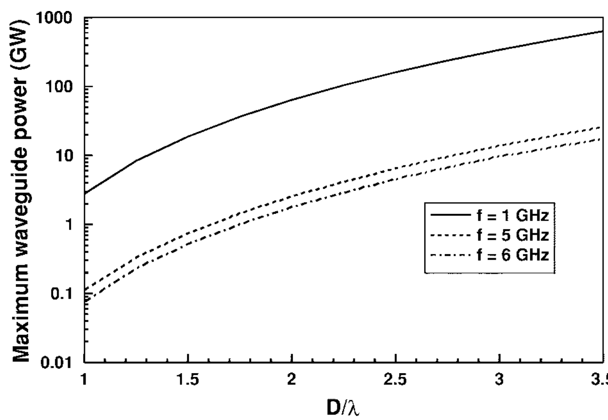

Fig. 1. Maximum TM$_{01}^{\odot}$ power supported by a smooth-walled waveguide as a function of D/λ, assuming $E_{\max} = 100$ kV/cm.

One method of increasing the power-handling capability of linear beam devices is to use an overmoded structure, increasing the diameter of the electrodynamic structure to several times a free-space wavelength. With this method, microwave-generating structures can be designed with resulting internal RF electric fields below critical field emission breakdown levels. Incorporating two-stage overmoded electrodynamic structures, two recent devices have produced record levels of multigigawatt microwave radiation. The relativistic diffraction generator (RDG) [3] has produced a peak output power of 4.5 GW in the 9–11.3-mm wavelength range and the multiwave Čerenkov generator (MWCG) [4] has produced 15 GW at a wavelength of 3 cm.

Fig. 1 demonstrates the advantages of the use of an overmoded structure for high-power generation. In the figure, we plot the maximum TM$_{01}^{\odot}$ power that can be supported by a smooth-walled waveguide (obtained by integrating the Poynting flux) assuming that the maximum allowable electric field at the wall is $E_{\max} = 100$ kV/cm. The curves are plotted as a function of the ratio of the guide diameter D to the guide wavelength λ for several frequencies. Consider, for example, the $f = 6$ GHz curve: at $D/\lambda = 1$, the waveguide supports a maximum propagating RF power of $P_{\max} \sim 77$ MW; increasing the guide diameter by only a factor of three results in $P_{\max} \sim 9.4$ GW, an increase of more than 120 fold in the guide's power-handling capacity.

However, while overmoded structures may beneficially reduce the internal RF electric fields in a device, detrimental consequences may also exist. These include multimode generation within the electrodynamic structure, spatial mode conversion in the transmission system and at system interfaces, and a general broadening of the frequency spectrum—all factors that can contribute to a decrease in the maximum RF power output and generation efficiency. These potential problems are difficult to treat either analytically or computationally, given the abundance of symmetric and nonsymmetric propagating modes in the overmoded system.

To study these potential problems and to further investigate the use of overmoded electrodynamic structures in HPM devices, we describe in this work a series of systematic experiments with overmoded $(D/\lambda \sim 3)$ backward-wave oscillators (BWO) in the 5.2–5.7-GHz frequency range. The BWO was chosen as a test vehicle because it possesses a number of attractive features, including high spectral purity, modest frequency tunability, and the ability to produce high-output power. In addition, its relatively simple single-stage electrodynamic structure facilitates modeling.

A key goal in the experiments was to demonstrate that a pure symmetric (fundamental) TM mode could be generated by such an overmoded device; particular attention was paid to the design of the electron gun, beam propagation system, and the electrodynamic structure hardware to ensure symmetry. The entire experimental system was extensively cold tested to accurately measure its electromagnetic characteristics before testing at full power. The generated microwave energy was radiated into a large anechoic chamber, where the radiation pattern was sampled and highly accurate frequency measurements were made. Section II contains a brief review of the physics of BWO's and describes the design methodology used to generate the electrodynamic structure dimensions. Section III discusses the specific characteristics of the experimental device. Section IV describes the experimental layout and diagnostics. Section V describes generation and propagation experiments with large diameter, annular, relativistic electron beams. Sections VI and VII describe HPM experiments at constant and varied axial magnetic fields, respectively. A summary of the results and conclusions is presented in Section VIII.

II. Design Methodology

In this section, we present a brief review of BWO physics, a discussion of the numerical design tools used to develop the experimental BWO structure and an outline of our design methodology. With the numerical tools, we conducted parametric studies of the BWO electrodynamic structure dimensions (average diameter and corrugation period and amplitude) and the electron-beam parameters (voltage, current, and beam diameter), culminating in the design of a sinusoidally corrugated structure of modular interlocking rings that enabled the electrodynamic structure length to be experimentally varied.

A. Brief Review of BWO Physics

Fig. 2 is a cross-section sketch of an overmoded BWO. The overmoded BWO shares many similarities with its conventional nonovermoded $(D/\lambda \sim 1)$ counterpart. Both devices consist of a thin, annular, axially streaming electron beam transported through a periodically corrugated electrodynamic structure (typically sinusoidal or semicircular in cross section in high-power devices); both devices are immersed in a strong axial magnetic field to constrain the motion of the electrons to one dimension.

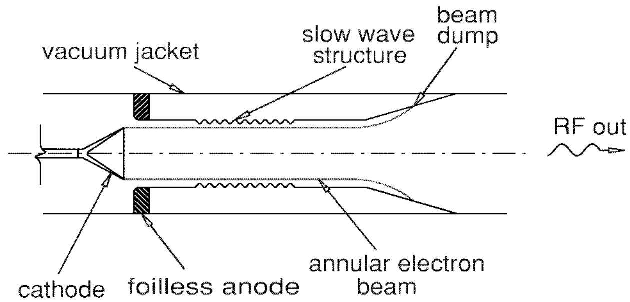

Fig. 2. Cross-section sketch of an overmoded backward-wave oscillator.

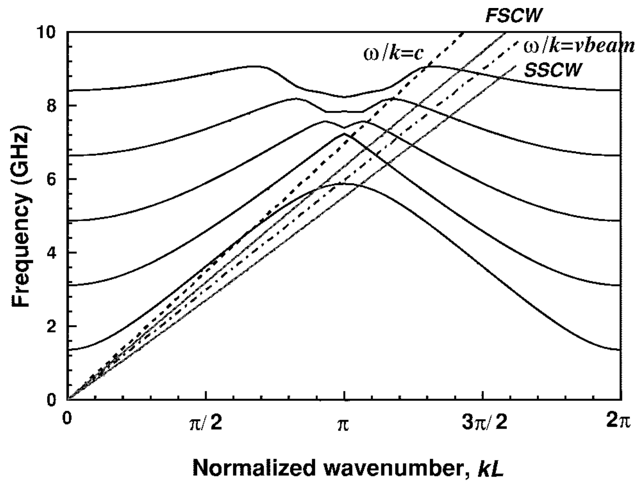

Fig. 3. Beam waves superimposed on the dispersion curves for the first five TM_{0n} modes in an empty sinusoidally corrugated structure.

In both devices, the periodic structure acts to slow the axial phase velocity of the electromagnetic waves to below the speed of light, where $TM_{0n}^{\odot}$ waves, which have a longitudinal electric field component E_z can interact with the axially streaming beam electrons. For low-current beams with negligible space charge, the condition for synchronism is $\omega \sim kv_{\text{beam}}$, where ω is the radian frequency, k is the axial wavenumber, and v_{beam} is the velocity of the beam electrons. For high-current beams, the beam-space charge induces longitudinal oscillations on the beam, which, in turn, interact with the longitudinal RF fields in the structure producing a fast- and slow-space charge wave (fast and slow relative to the $\omega = kv_{\text{beam}}$ beam line). The slow-space charge wave (SSCW) is excited by the extraction of RF energy from the beam's kinetic energy; this is the interaction of interest for microwave generation. For a BWO, the design goal is to create a structure where the SSCW synchronously interacts with the negative group velocity $(\partial\omega/\partial k < 0)$ spatial harmonic of the $TM_{01}^{\odot}$ wave.

Fig. 3 is a sample dispersion plot of a beam in an infinite periodically corrugated electrodynamic structure. The radian frequency ω is plotted as a function of the normalized wavenumber kL, where L is the length of a single corrugation period. In the figure, the first five symmetric $TM_{0n}^{\odot}$ waves are plotted along with the $\omega = kc$ speed-of-light line, the $\omega = kv_{\text{beam}}$ beam line, and the fast- and slow-space charge waves.

Several key attributes distinguish an overmoded BWO from a nonovermoded BWO. The most obvious difference is the diameter of the electrodynamic structure. In addition to increasing the device's power-handling capability, the larger diameter structure and small corrugation amplitude cause the RF waves to propagate as surface waves, with the highest fields close to the walls [5]. To maximize the beam-wave interaction, the diameter of the electron beam is correspondingly large in an overmoded BWO, typically, 85–95% of the average diameter of the structure. In contrast, RF waves in a nonovermoded BWO propagate as volumetric waves and the beam diameter-to-wall ratio is proportionally smaller. Another distinguishing feature of the overmoded BWO is the amplitude of the periodic corrugations that make up the electrodynamic structure. In an overmoded BWO, the corrugation amplitude is small, typically, $\leq$10% of the average structure radius compared with $\sim$30% in a nonovermoded BWO.

B. Development of Numerical Design Tools

In the absence of a fully developed theory of overmoded BWO operation, we made some simplifying assumptions and developed a set of numerical tools to assist us in the design of the experimental overmoded BWO hardware. Using the assumptions described below, we modeled the beam-wave interaction by superimposing the linear dispersion curves for an annular beam in an infinite smooth-walled waveguide on the cold-structure (no beam) $\mathrm{TM}_{0n}^{\odot}$ dispersion curves for an infinite corrugated wall structure with the same average radius. Although an approximation, this technique is computationally fast, enabling us to rapidly generate parametric studies of the effect of variations of structure dimensions and beam parameters on the beam-wave interaction frequency. This technique was quite successful, as discussed in the experimental results section of this paper.

To simplify computation, we made two key assumptions based on attributes of overmoded linear beam devices. First, we assumed that the beam dispersion in the overmoded periodic structure could be reasonably approximated by the beam dispersion in a smooth-walled waveguide with a radius equal to the average radius of the periodic structure. This assumption was justified by the observation that overmoded slow-wave devices tend to have small corrugation amplitudes. Second, we assumed that the presence of the beam would not significantly modify the cold-structure (no beam) electromagnetic fields, and, thus, frequency pulling effects could be ignored. (Referring to the dispersion plot of Fig. 3, we assumed that while the beam current was large enough to create beam space charge waves, it was not large enough to modify the shape of the cold-structure $\mathrm{TM}_{01}^{\odot}$ dispersion curve.)

We justified the latter assumption by considering the ratio of the beam current to the space charge limiting current (I_b/I_{SCL}) as a measure of the relative importance of beam-space charge. In a smooth-walled waveguide, the space-charge limiting current I_{SCL} is related to the guide radius r_0 and the beam radius r_b by [6]–[8]

$$I_{\mathrm{SCL}} = \frac{I_A}{2\ell n(r_0/r_b)}(\gamma_c^{2/3}-1)^{3/2}\ \mathrm{kA} \tag{1}$$

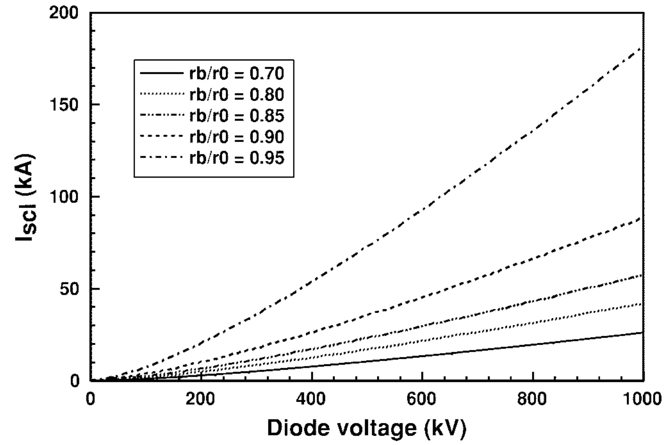

Fig. 4. Space-charge limiting current as a function of cathode potential for various ratios of beam-to-waveguide radii.

where $I_A = 17.1$ kA is the Alfvén current, $\gamma_c = 1 + |e\phi_c/m_e c^2|, e/m_e$ is electron charge-to-mass ratio, and ϕ_c is the cathode potential. For ratios of $r_b/r_0 \approx 1$, I_{SCL} is on the order of 100 kA (Fig. 4), much larger than the operating current of the experiment. Referring to the figure, if $r_b/r_0 \geq 0.85$, then, for most of the parameters of our experiment, $I_b/I_{\mathrm{SCL}} \leq 15\%$. Based on this relatively low ratio, we chose to simplify our computational tasks and assumed that the beam-space charge did not significantly modify the cold-structure fields.

Following [6] and [7], the dispersion relation for a beam propagating in a smooth-walled waveguide was obtained assuming an infinitesimally thin beam one-dimensional (1-D) motion of the electrons and symmetric $\mathrm{TM}^{\odot}$ time-harmonic fields. The dispersion relation, relating the radian frequency and the axial wave number, can be expressed as

$$J_\ell(\Gamma r_0) + \left(\frac{\pi I_b}{\beta_b\gamma_b^3 I_A}\right)\left(\frac{\Gamma c}{\omega - k v_b}\right)^2 \times J_\ell(\Gamma r_b)[J_\ell(\Gamma r_b)N_\ell(\Gamma r_0) - J_\ell(\Gamma r_0)N_\ell(\Gamma r_b)] = 0 \tag{2}$$

where $\Gamma = [(\omega/c)^2 - k^2]^{1/2}, v_b$ is the beam velocity, $\beta_b = v_b/c$, $\gamma_b = 1 + |e\phi_b/m_e c^2|$, and ϕ_b is the depressed beam potential.

Following [9], the cold-structure dispersion curves for an infinite, sinusoidally corrugated structure were obtained by transforming the $\mathrm{TM}_{0n}^{\odot}$ mode Maxwell's equations and the appropriate boundary conditions into a system of coupled linear differential equations whose coefficients are a function of the periodically varying wall radius and its derivative. This system of coupled linear differential equations with periodic coefficients was then converted to a matrix eigenvalue problem by the application of Floquet's theorem and by expanding the periodic parts of the Floquet solution in a Fourier series. The eigenvalue problem was solved numerically using standard computational techniques [10].

Using the analytic techniques described in the previous paragraphs, we developed codes to conduct parametric studies of overmoded BWO designs. We used these codes to assess the effects of varying overmoded BWO parameters such as

TABLE I
ELECTRON BEAM PARAMETERS

Cathode Voltage Range	250 kV $\leq \phi_c \leq$ 900 kV
Beam Current Range	2 kA $\leq I_b \leq$ 20 kA
10–90% Risetime	$\sim$ 60 ns
Flat Top	$\sim$ 80 ns
Axial Magnetic Field	0 kG $\leq B_z \leq$ 14 kG

the electrodynamic structure diameter, the corrugation period and amplitude, the beam diameter, and the beam voltage and current. Fig. 3 is an example of the output from our design codes.

III. DESIGN OF A G-BAND OVERMODED SLOW-WAVE STRUCTURE

To study the feasibility of using overmoded electrodynamic structures for HPM generation, we designed a set of overmoded BWO hardware to produce HPM radiation in the frequency range of 5–6 GHz. The average diameter of the structure was 16.88 cm, corresponding to a $D/\lambda \sim 3$. As shown in Fig. 1, this guide-diameter-to-wavelength ratio should conservatively support propagating RF fields with powers in excess of 9 GW.

The experiment was driven by the Army Research Laboratory's (ARL) TEMPO electron-beam accelerator [11], a single-shot accelerator capable of producing an 80 ns duration (flat top) electron beam in the voltage range of 250–900 kV with a corresponding beam current of 2–20 kA. The beam was immersed in a strong axial magnetic field produced by pulsed-field coils; the pulse duration was far in excess of the magnetic diffusion time through the experimental structures. The electrical parameters are summarized in Table I.

The overmoded BWO had to meet the following design criteria: 1) the interaction frequency range must fall within 5 GHz $\leq f \leq$ 6 GHz; 2) the interaction range should be close to the edge of the passband of the $TM_{01}^{\odot}$ mode (to provide data for comparison with nonlinear models under development); and 3) the frequency separation between the $TM_{01}^{\odot}$ and $TM_{02}^{\odot}$ modes should be as large as possible to minimize the chance of exciting higher order modes.

With the average structure diameter set at $d_{\text{avg}} = 16.88$ cm, the desire to operate near the $kL = \pi$ point on the dispersion curve, and the beam-electrical parameters constrained by the accelerator, the remaining free parameters in the design were the electrodynamic structure's corrugation period and amplitude and the diameter of the electron beam. The amplitude and periodicity of the corrugations affect the BWO cutoff frequencies and the extents of the frequency passbands and stopbands. The radial position of the beam affects the frequency of interaction and the strength of the beam-wave interaction. (Without a self-consistent beam-wave model to guide us, the beam radius was set at ~87% of the average guide radius—a compromise between good beam-wave coupling and a beam diameter that could be experimentally collimated and reliably transported over a 1-m distance without losses to the walls.)

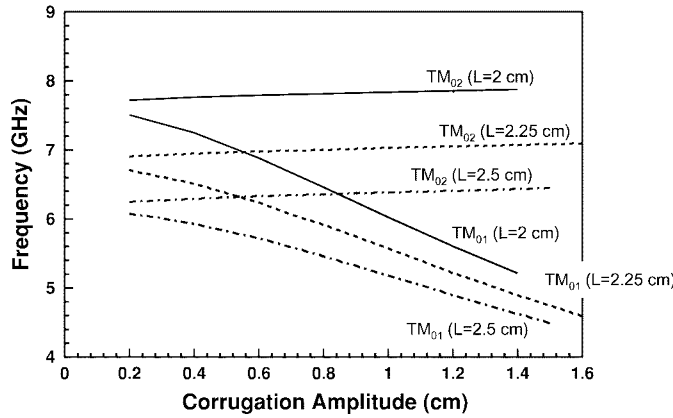

Fig. 5. Frequency separation at $kL = \pi$ of the $TM_{01}^{\odot}$ and $TM_{02}^{\odot}$ modes for $R_{\max} = 7.7$ cm and variable corrugation amplitudes and periods.

TABLE II
PHYSICAL DIMENSIONS OF THE ELECTRON BEAM AND SINSUOIDALLY CORRUGATED SLOW-WAVE STRUCTURE

SWS Maximum Radius	8.89 cm
SWS Mininum Radius	7.99 cm
SWS Period	2.15 cm
Average Beam Radius	7.375 cm
Beam Thickness	$\sim$ 2 mm

Using the design tools developed in Section II-B, we performed a series of broad parametric studies to obtain a first-order estimate of the size of the corrugation amplitude and period. The results of these studies indicated that a corrugation (peak-to-peak) amplitude of 0.5 cm $\leq \delta \leq$ 1.5 cm and a period of 2.0 cm $\leq L \leq$ 2.5 cm would produce radiation in the 5–6-GHz range.

A more detailed set of parametric studies sought to minimize the possibility of multimode generation by maximizing the widths of the stopbands on the dispersion plots. Fig. 5 is a plot of the frequency separation between the $TM_{01}^{\odot}$ and $TM_{02}^{\odot}$ modes at the $kL = \pi$ point on the dispersion diagram for the case of a maximum structure radius of $R_{\max} = 7.7$ cm. The frequency separation increases as the corrugation amplitude increases and the corrugation period decreases. Referring to the figure, an amplitude $\delta = 1$ cm and a period $L = 2$ cm yield a $TM_{01}^{\odot}$–$TM_{02}^{\odot}$ frequency separation of almost 2 GHz. This combination of frequency separation and structure dimensions was deemed near optimum for the experiment.

With some additional analysis and fine tuning of the beam parameters, the design of the electron-beam system and overmoded, sinusoidally corrugated electrodynamic structure was finalized. Table II summarizes the physical dimensions of the beam and the structure. The calculated range of accessible frequencies (given the range of available TEMPO beam voltages and currents) is shown in Fig. 6, which plots the SSCW's for the extremes of beam parameters on the cold-structure $TM_{0n}^{\odot}$ dispersion curves.

The sinusoidal slow-wave structure (SWS) was fabricated from 304 stainless steel as a modular set of interlocking rings (Fig. 7) to allow us to study the effects of variations in the

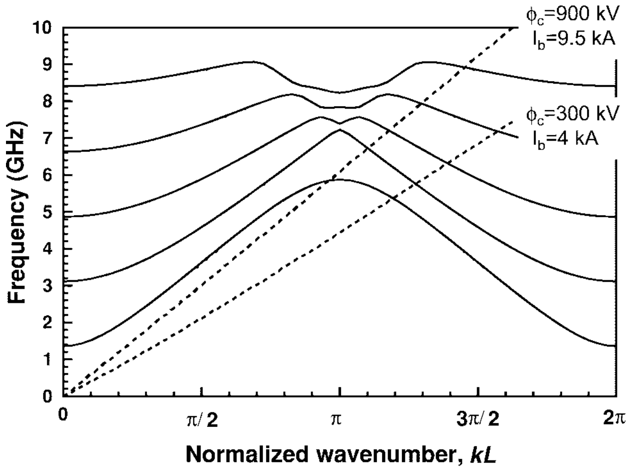

Fig. 6. Calculated interaction range for the overmoded BWO experiments.

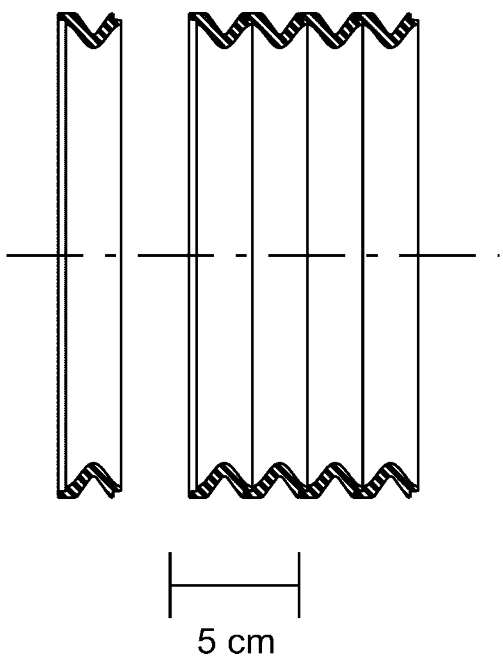

Fig. 7. Modular sinusoidally corrugated SWS.

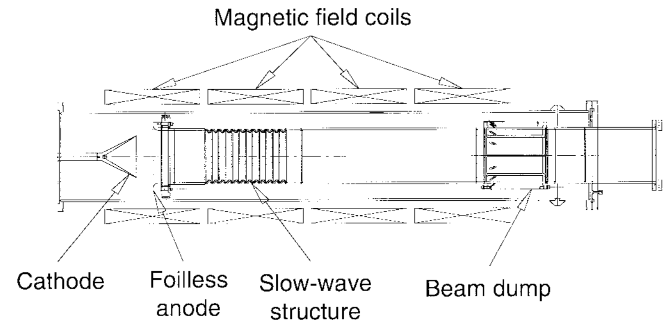

Fig. 8. Detail of the magnetized microwave interaction region.

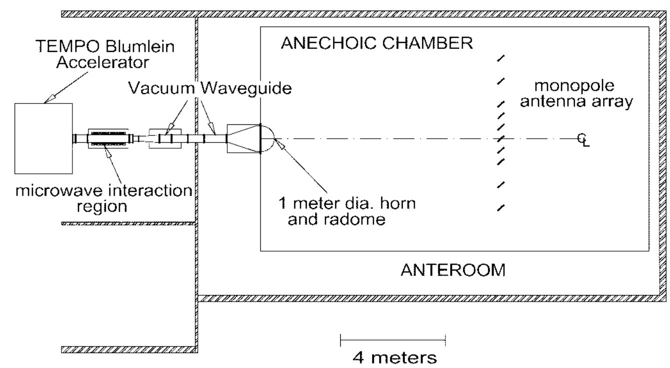

Fig. 9. Overmoded BWO experiment layout.

length of the electrodynamic structure. With these rings, the structure could be varied in length from a single period up to 35 periods.

Fig. 8 is a detailed drawing of the experimental magnetized microwave interaction region, including the annular explosive emission cathode, foilless carbon anode, modular electrodynamic structure, and electron beam collector. The diode and interaction regions are immersed in a strong axial magnetic field provided by a set of four pulsed-field coils.

IV. Experimental Layout and Diagnostics

Fig. 9 is a layout of the entire experiment. The major subsystems are the TEMPO electron-beam accelerator, the magnetized microwave interaction region (described in the previous section), a long waveguide transmission system consisting of a linear uptaper and approximately 3 m of 29.2-cm-diameter straight cylindrical guide, a 1-m-diameter output horn with an axial length of 1.03 m, and a hemispherical radome. The large diameter horn was chosen to minimize the chance of breakdown due to high fields at the air-vacuum interface. The system was evacuated to a residual gas pressure of 10^{-6}–10^{-5} Torr. The horn radiated into a large (15 m L × 9 m W × 7.5 m H) anechoic chamber.

The electron-beam diagnostics consisted of a capacitive voltage divider to monitor the cathode voltage and four B-dot loops azimuthally spaced at 90° intervals directly upstream of the foilless carbon anode.

The principal microwave diagnostics consisted of a seven- to ten-element array of calibrated short-monopole receiving antennas and a pair of cross-polarized (vertical and horizontal) WR137 standard gain horns. The short-monopole was selected as the receiving antenna for its relatively flat frequency response in the 5–6-GHz band and low directivity (making it relatively insensitive to angular orientation). The monopoles were oriented at an angle of ∼45° with respect to the centerline of the experiment and were positioned so as to detect horizontally polarized radiation. The cross-polarized horns were located 9.19 m from the plane of the large output horn. The receiving antennas were individually calibrated on an antenna range as well as *in situ* in the anechoic chamber.

Before the beam-driven high-power tests, we carefully studied the $TM_{01}^{\odot}$ transmission characteristics of the vacuum waveguide system and the antenna and radome at low power to identify potential sources of passive spatial-mode conversion. As discussed in the Appendix, although we tried to minimize internal reflections in the system, there were sufficient reflections from joints in the vacuum waveguide sections and the antenna radome to induce substantial asymmetries in the radiated pattern. These asymmetries were sensitive to <10-MHz changes in frequency. However, despite these pattern asymmetries, we were able to develop a pattern-integration technique (described in the Appendix) that enabled us to compute source powers that agreed to within ±1 dB of a measured magnetron calibration source over the frequency range of interest.

Once calibrated, the monopole array enabled us to measure a 1-D slice of the radiation pattern in a single shot. The microwave radiation was detected with calibrated 0.1–18-GHz detector diodes and the frequency was accurately measured with a two-channel heterodyne technique. With this technique, a received microwave signal was split and channeled into two double-balanced mixers, each driven by its own unique local oscillator (LO) frequency. The radiated microwave frequency could then be unambiguously determined from the resulting two intermediate frequency (IF) signals.

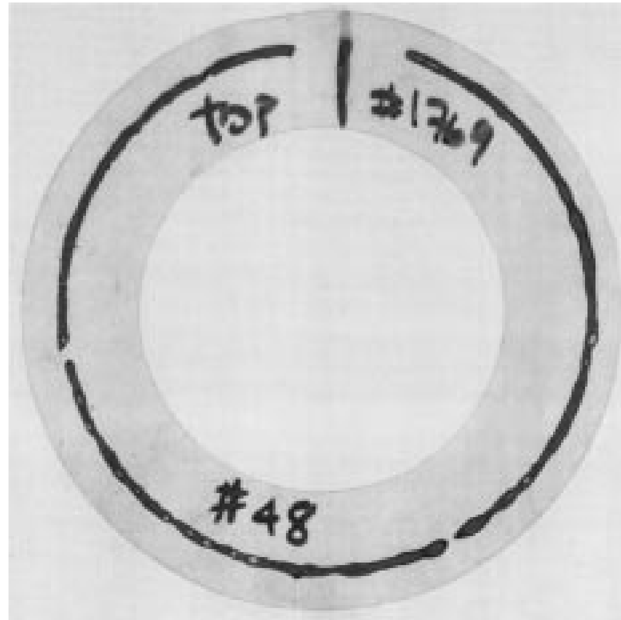

(a)

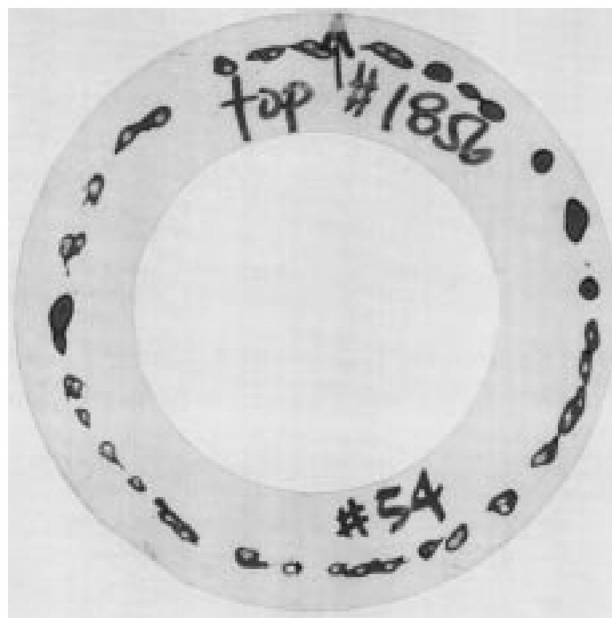

(b)

Fig. 10. Thermal-damage patterns for (a) an electron beam generated with a coated cathode ($\phi_c = 608$ kV, $I_b = 10.5$ kA) and (b) an electron beam generated with an uncoated cathode ($\phi_c = 591$ kV, $I_b \simeq 10$ kA).

V. Generation and Propagation of Large-Diameter Annular Electron Beams

Before the HPM generation experiments, we conducted extensive studies of large-diameter annular electron beams. The goal of these experiments was to eliminate asymmetries in the electron beam that could contribute to multimoding in the microwave experiments.

The electron beam was generated from an explosive emission cathode that was fabricated from 304 stainless steel. The shape of the cathode (optimized experimentally) maximized the electron emission from the cathode surface while minimizing emission from the cathode frustum surface and the cathode shank. The beam was propagated down a smooth-walled guide and collimated by a strong (up to 14 kG) axial magnetic field.

The beam voltage was measured with a capacitive voltage divider. The beam current as a function of axial position was measured with a series of B-dot loops set at fixed longitudinal intervals down the smooth-walled guide. The beam uniformity was measured with beam-induced thermal-damage patterns and X-ray pinhole camera diagnostics. The beam rotation was measured by using a thick aluminum target to fully intercept a segment of the beam and then varying the axial distance of the intercepting target from a thermal-damage pattern target on successive shots. No beam rotation was observed in any of the experiments.

We developed a novel carbon-epoxy cathode coating, which gave us azimuthally uniform electron emission over a wide range of average electric fields, 60 kV/cm $\leq E_z \leq 600$ kV/cm, with corresponding cathode current densities of 350 A/cm^2 $\leq J \leq$ 1600 A/cm^2. The coating consisted of extremely fine graphite powder (for good field enhancement) suspended in epoxy, which was applied to the annular emitting area of the stainless-steel cathode and subsequently machined flat. Fig. 10(a) and (b) are thermal-damage patterns for similar voltage and current beams generated with a coated and uncoated cathode, respectively. As can be seen in the figures, the uncoated cathode is highly filamented, while the coated cathode displays good beam uniformity (the gaps in the coated cathode beam damage pattern are due to the presence of obstructing targets).

Because of the electron beam studies, we produced cathode designs capable of generating symmetric beams suitable for use in the overmoded BWO experiments. We generated thin (∼2 mm) nonrotating annular electron beams with good symmetry and azimuthal uniformity and successfully propagated these large-diameter beams (up to 95% of the guiding structure diameter) over axial distances of up to 1 m. The beams were stable and symmetric over the voltage and current range of the experiment (see Table I) and could be suitably collimated

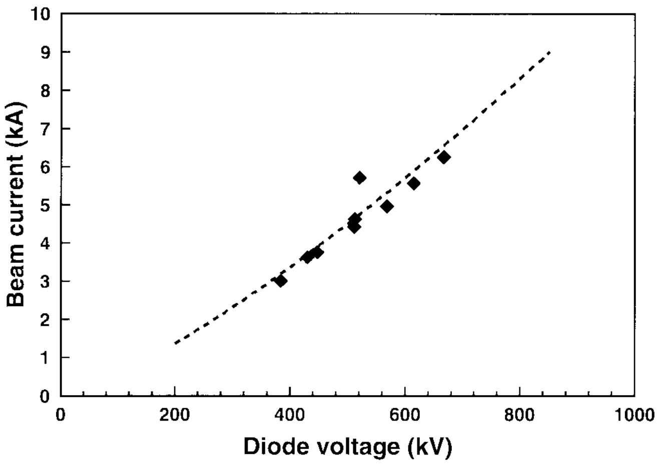

Fig. 11. Beam current versus accelerating potential for a diode with an A-K gap of 4 cm and a 13.93-cm-diameter annular (∼2-mm-thick) cathode. The dotted line represents a numerical fit through the data, where I_b(kA) $= (1.4 \times 10^{-3})\phi_c^{1.30}$(kV).

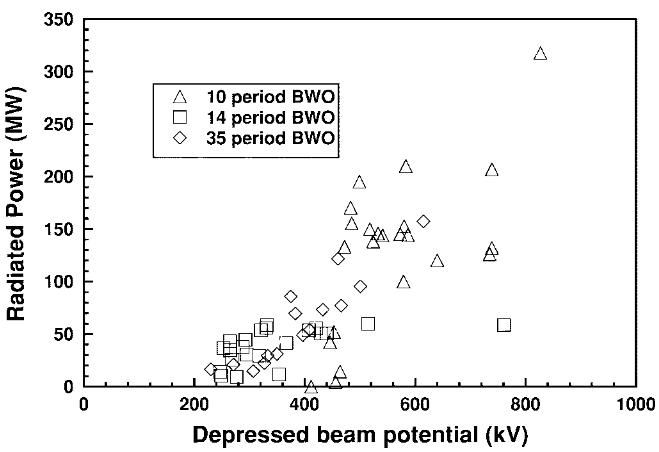

Fig. 12. Radiated microwave power versus depressed beam potential for the 10-, 14-, and 35-period sinusoidal BWO structures.

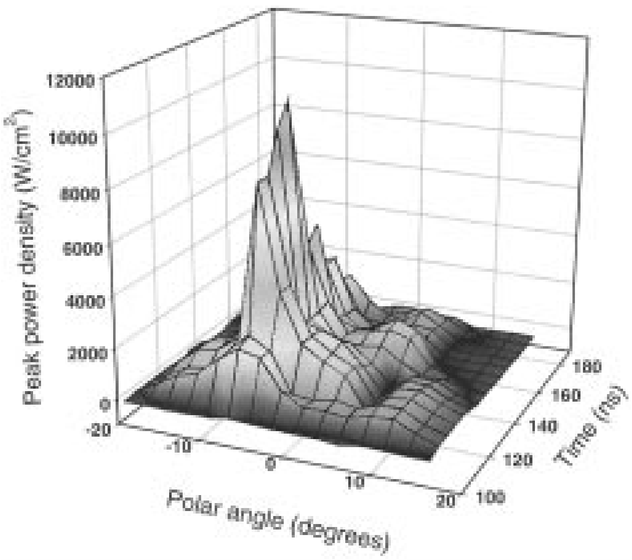

Fig. 13. Radiated microwave power density at $R = 9.19$ m as a function of time and polar angle (ten-period BWO).

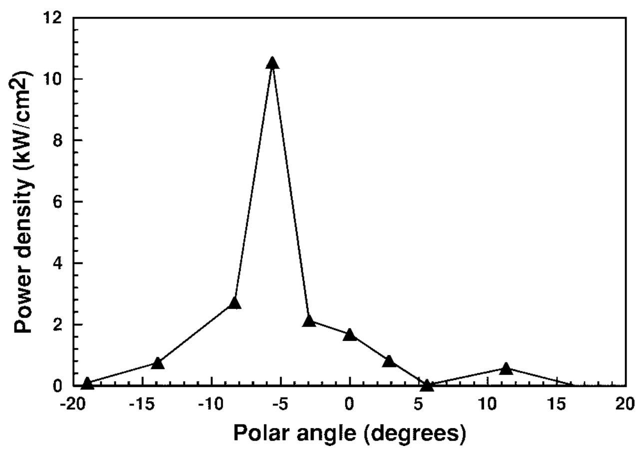

Fig. 14. Discretely detected power density at $R = 9.19$ m versus polar angle for time $t = 133.5$ ns (ten-period BWO).

within the available range of axial magnetic field strengths. Fig. 11 is an example of the dependence of the beam current on the accelerating potential for the large diameter diodes used in the overmoded BWO experiments.

VI. Microwave Generation Experiments at a Constant $B_z = 10$ kG

In this section, we describe the results of overmoded $(D/\lambda \sim 3)$ BWO experiments with sinusoidally corrugated structures with lengths of 8, 10, 14, and 35 periods. The range of cathode accelerating potentials was $220 \text{ kV} \leq \phi_c \leq 905$ kV with a corresponding beam-current range of $2.2 \text{ kA} \leq I_b \leq 9.0$ kA. The experiments were conducted at a spatially uniform axial magnetic field strength of $B_z = 10 \pm 0.2$ kG.

The experimental measurements and subsequent nonlinear modeling strongly indicate that the experiment generated pure $TM_{01}^{\odot}$ mode radiation. Although (as expected) the radiation patterns exhibited asymmetries, the measurements of frequency and wave polarization along with good agreement with theory make a strong case that a single symmetric mode was produced. This assertion is further enhanced when combined with the results of Section VII, which takes finite magnetic field effects into account.

A. Measurements of Radiated Microwave Power

Fig. 12 plots the measured radiated microwave power from a 10-, 14-, and 35-period structure as a function of (calculated) depressed beam potential. No radiation was observed from the eight-period structure for the range of experimental beam voltages and currents.

A maximum RF power of ∼320 MW was generated with a ten-period structure. The beam voltage and current was 827 kV and 9.0 kA, respectively, with a corresponding RF power generation efficiency of about 4%. The measured time and spatial evolution of the power density radiated into the anechoic chamber at a range of 9.19 m is plotted in Fig. 13.

The 320-MW shot had a measured peak-power density of 10.5 kW/cm^2 at a time $t = 133.5$ ns into the voltage pulse. Fig. 14 is a plot of a 1-D slice of the spatial pattern for this time. As can be seen in the figure, the spatial

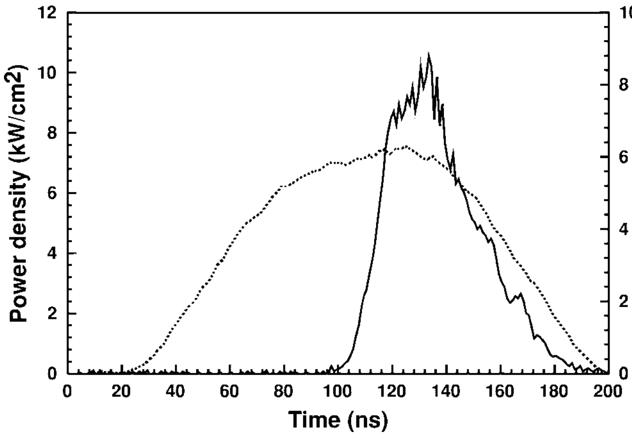

Fig. 15. Typical microwave pulse duration plotted on top of a beam current (dotted line) versus time curve.

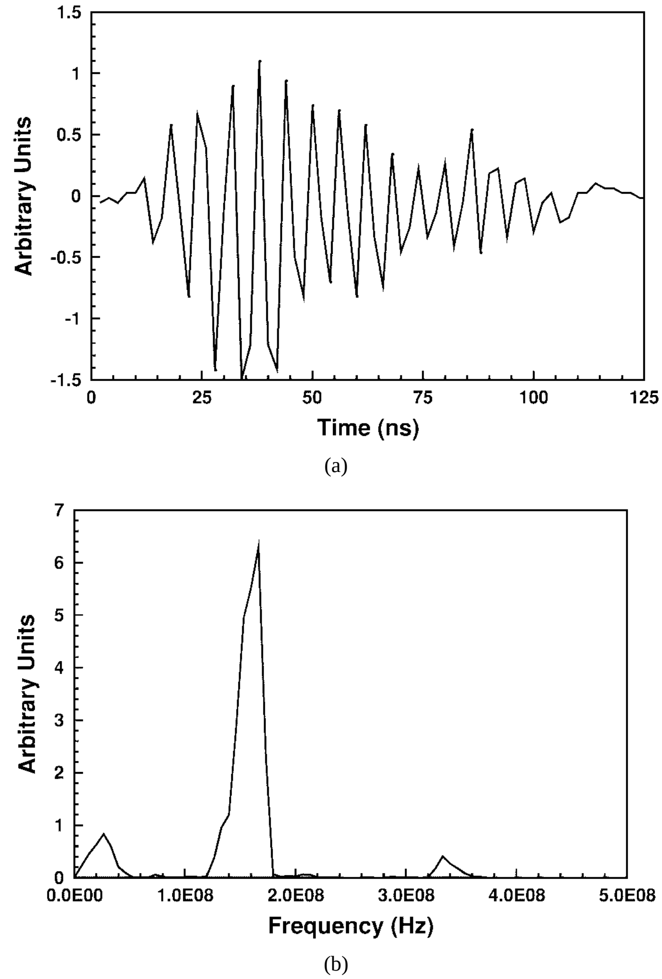

Fig. 16. (a) IF signal from 320 MW ten-period BWO shot (LO = 5.65 GHz) and (b) the corresponding FFT of the IF signal.

pattern exhibits asymmetries similar to those observed in the magnetron calibration tests (see Fig. 24 in the Appendix).

Pulse shortening due to internal breakdown was not observed in any of the shots. In general, the microwave pulse remained on as long as the electron beam contained sufficient power to drive the instability. Fig. 15, which superimposes a plot of microwave power density versus time on a beam-current curve, is typical for the shots that produced microwaves.

B. Frequency Measurements

As discussed in Section IV, a two-channel heterodyne technique was used to obtain highly accurate (±0.1%) measurements of the radiated microwave frequency in the anechoic chamber. The estimated error for these measurements is ±3 MHz, slightly larger at the lowest beam voltages where the nonoscillating region is approached.

The IF waveform for the 320-MW (10–period BWO) shot is shown in Fig. 16(a); the corresponding fast Fourier transform (FFT) of the IF signal is plotted in Fig. 16(b). The LO frequency was 5.65 GHz, resulting in a measured operating frequency of 5.483 GHz. As can be seen in the figures, the microwave radiation is highly coherent, with a $\Delta f/f = 0.45\%$. Such spectral purity was typical of the 10- and 14-period BWO experiments—the majority of microwave-producing shots had a $\Delta f/f < 0.5\%$. The spectral purity of the 35-period experiments was difficult to measure because of noise problems in the diagnostics system.

We looked for the presence of higher order modes by making heterodyned frequency measurements with LO frequencies corresponding to the next higher order ($TM_{02}^{\odot}$) symmetric mode interaction. No significant power was observed at frequencies above those corresponding to fundamental $TM_{01}^{\odot}$ mode interaction.

C. Measurements of Wave Polarization

The RF wave polarization was measured by a pair of cross-polarized WR137 standard gain horns located slightly above the experiment centerline at a distance $R = 9.19$ m. The power P received by the horns is proportional to the square of the magnitude of the incident electric field

$$P_{\perp} \propto E^2 \sin^2 \theta_{\mathrm{pol}}$$
$$P_{\|} \propto E^2 \cos^2 \theta_{\mathrm{pol}} \qquad (3)$$

where θ_{pol} (the polarization angle) is measured with respect to the horizontal axis of the experiment with the positive sense defined in the counterclockwise direction emanating from the source. From (3), the polarization angle is

$$\theta_{\mathrm{pol}} = \arctan\left(\sqrt{\frac{P_{\perp}}{P_{\|}}}\right). \qquad (4)$$

As an example, the measured wave polarization as a function of time is plotted in Fig. 17 for the 320 MW (ten-period BWO) shot. This curve was typical for the 10- and 14-period BWO shots. As can be seen in the figure, the polarization versus time is relatively constant (~63° ± 9°) and free of structure over the duration of the microwave pulse (115 ns $\leq t \leq 150$ ns, 3-dB pulse width). If multiple modes or mode hopping were present, one would expect greater excursions in the polarization angle as a function of time.

In Fig. 18, the measured (average) polarization angles versus frequency for the 10- and 14-period BWO shots are compared with the measured polarization angles from the

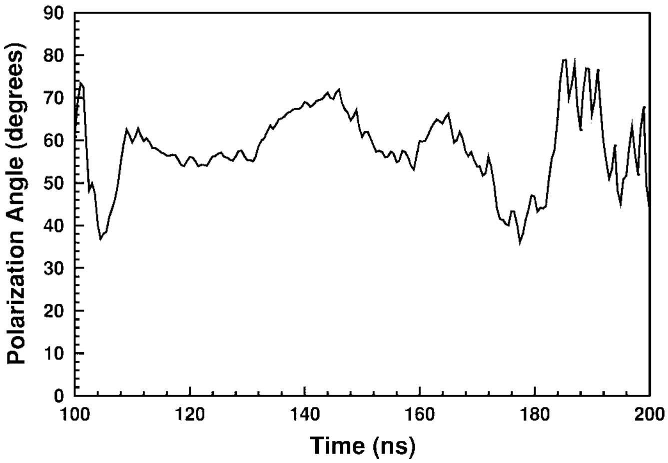

Fig. 17. Wave-polarization angle as a function of time for the 320-MW ten-period BWO shot.

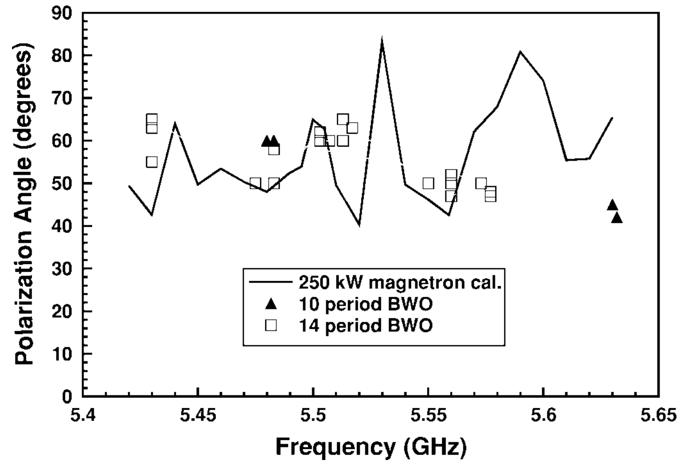

Fig. 18. Average polarization angle as a function of frequency for 10- and 14-period BWO structures with 250-kW magnetron system calibration measurements.

250-kW magnetron system calibrations. The experimental and calibrated angles are in relatively good agreement. When this observation is considered along with the temporal stability of the polarization angle (e.g., Fig. 17) and the measured spectral purity of the radiation [e.g., Fig. 16(b)], the data strongly indicate that the experiments produced pure stable $TM_{01}^{\odot}$-mode radiation. As will be seen in the next two sections, subsequent nonlinear modeling supports this hypothesis.

D. Comparison of Experimental Results with Nonlinear Theory

The data from the experiments were used to validate a nonlinear theory of BWO operation. The nonlinear model, described in [12], is particularly relevant as it describes BWO operation near the edge of the stopband (the $kL = \pi$ point in Fig. 3), precisely the region of operation of our experiments (see Fig. 6).

In the nonlinear model, the cold-structure dispersion relation is approximated as a quadratic function of the wavenumber k. The interaction between the electron beam and the electromagnetic waves of the cold SWS is assumed to be weak. Over an axial length of a single period of the structure, the electromagnetic fields are assumed to have a spatial and temporal dependence identical to the cold-structure fields; the presence of the electron beam causes the envelope of the electromagnetic fields to vary slowly in time and axial distance. Reflections at the ends of the SWS are self-consistently accounted for with the appropriate boundary conditions on the slowly varying amplitude function describing the envelope of the electromagnetic fields. Electron motion is confined to one dimension by the assumption of an infinitely strong axial magnetic field.

Fig. 19(a)–(c) plots the experimentally measured frequency as a function of cathode potential, along with predictions made by the cold-structure approximation (Section II-B) and analyzes using the nonlinear BWO model. As can be seen in the figures, the experimentally measured frequency curves exhibit a tendency toward flatness with increasing beam potential. This trend is consistent with our original design analyzes using the decoupled beam and cold-structure dispersion curves, where the design interaction frequencies clustered around the π point of the $TM_{01}^{\odot}$-dispersion curve (Fig. 6). The trend is the result of two competing effects: on the one hand, increasing the diode potential raises the beam-wave interaction point higher in frequency toward the π point; however, in this experiment, the diode voltage and current could not be varied independently, but rather followed a modified Child's law with $I_b \propto \phi_c^{\alpha}$ $(1.3 \leq \alpha \leq 1.5)$. Thus, an increase in the diode potential is accompanied by an increase in beam current and an attendant increase in beam-space charge depression, which tends to lower the interaction frequency. For the range of experimental beam voltages and currents, the two competing effects tended to cancel each other out, resulting in a flat frequency versus diode voltage response.

The frequency shift between the cold-structure approximation and the experimental frequency curves is due to the fact that the approximation assumes no coupling between the beam and cold-structure fields, allowing for no modification of the dispersion curve by the beam space charge.

As reported in [12], the results of the nonlinear analyses also exhibit the same tendency toward asymptotic flatness with increasing beam potential. Agreement between the model and the experimental data improves with increasing SWS length. A possible explanation may be that the slowly-varying envelope approximation used in the nonlinear theory is not a valid assumption for SWS's that are short compared to their diameter—the ratio of SWS length to the average structure diameter is ~1.3 and ~1.8 for the 10- and 14-period structures, respectively, while it is ~4.5 for the 35-period structure.

The assumption of an infinite axial magnetic field may be another reason for the discrepancies between the measured data and the nonlinear calculations. At an axial magnetic field of $B_z = 10$ kG, the electron motion may not be 1-D as assumed in the model. As shown in the next section, the nonlinear model exhibits even better frequency agreement with the experiment when the effect of a finite axial magnetic field is included.

Reference [12] also made comparisons of experimental and theoretical peak efficiencies. The plots are reproduced

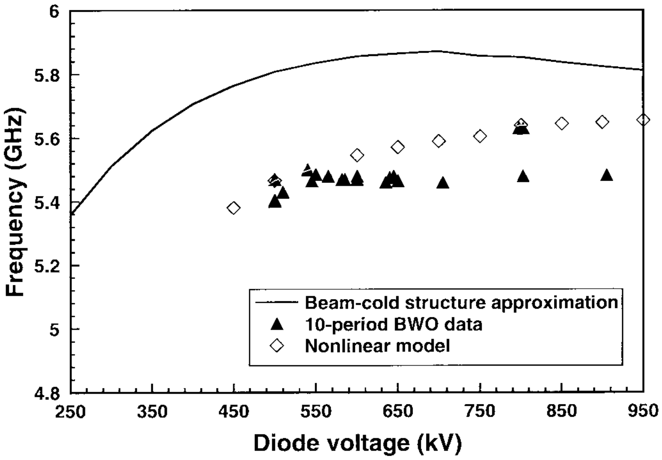

(a)

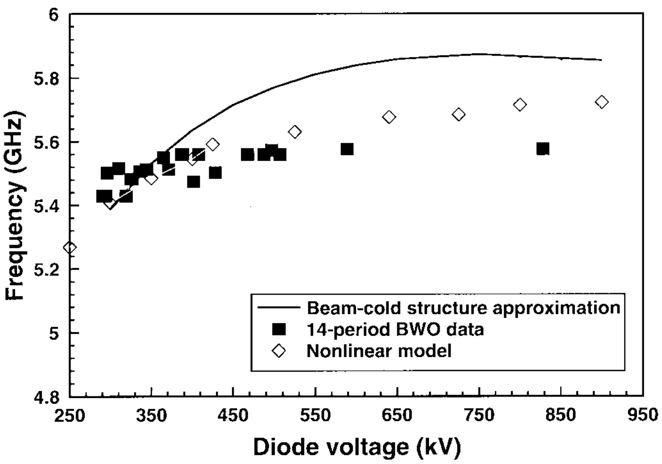

(b)

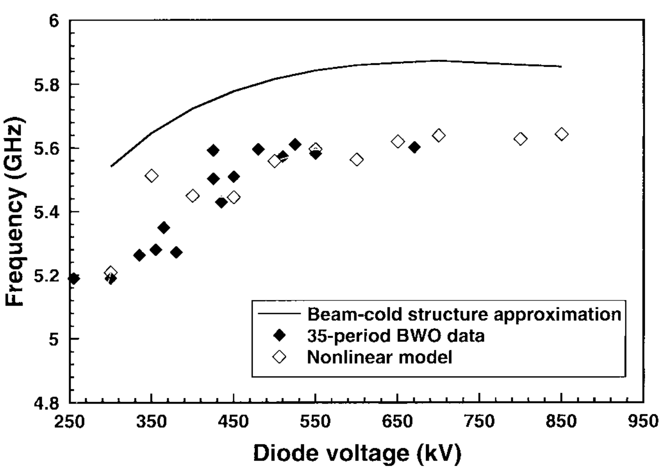

(c)

Fig. 19. BWO interaction frequencies versus cathode potential (measured data, cold-structure approximations, and nonlinear model calculations) for (a) 10-period, (b) 14-period, and (c) 35-period structures.

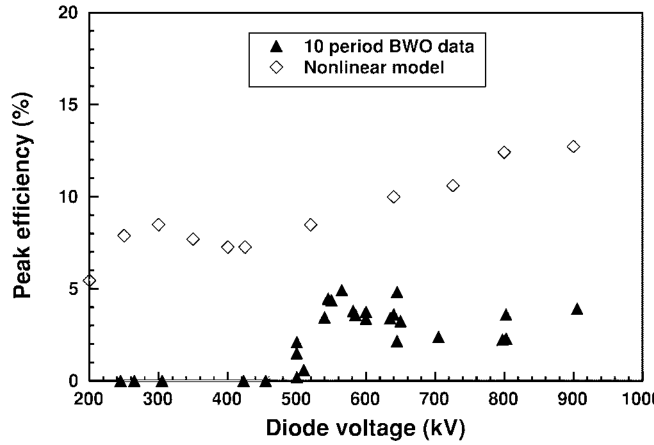

(a)

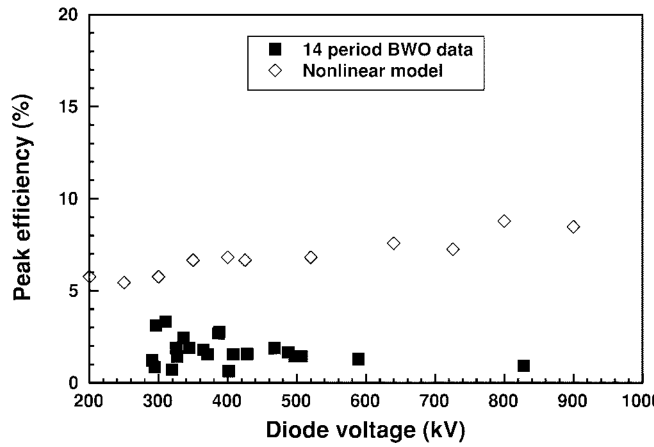

(b)

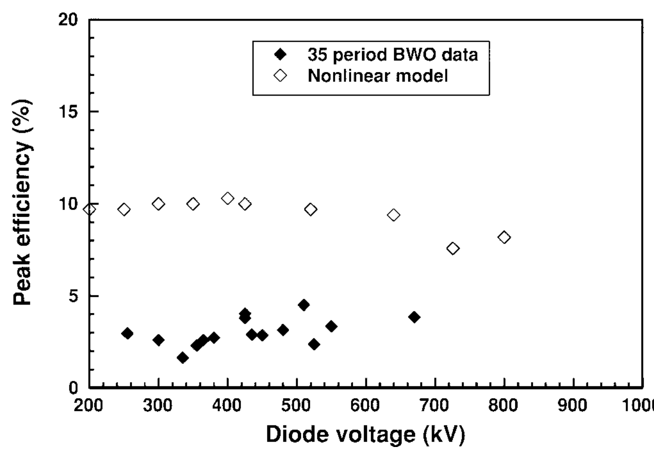

(c)

Fig. 20. BWO peak efficiencies versus cathode potential (measured data and nonlinear model calculations) for (a) 10-period, (b) 14-period, and (c) 35-period structures.

in Fig. 20(a)–(c) for completeness. While both the theoretical and experimental curves follow the same trend of relatively constant efficiency as a function of cathode voltage, there is poor agreement between the magnitudes of the measured and calculated efficiencies. As can be seen in the figures, the experimental efficiencies range from 3% to 5%, while the numerically calculated efficiencies range from 5% to 13%. The primary reason for the discrepancy between the measured and calculated efficiencies is probably the uncertainty in the measured radiated power, as discussed in Section IV and in the Appendix. It has also been suggested in [12] that the experiment may have generated higher order symmetric modes (particularly $TM_{02}^{\odot}$ and/or $TM_{03}^{\odot}$), which are not accounted for

TABLE III
BEAM AND FIELD SUMMARIES FOR VARIABLE B_z EXPERIMENTS

No. of Periods	Cathode Potential (kV)	Beam Current (kA)	B_z (kG)
10	$571 \pm 10\%$	$6.9 \pm 10\%$	$3.3 \leq B_z \leq 12.5$
14	$550 \pm 10\%$	$7.3 \pm 10\%$	$2.6 \leq B_z \leq 13.5$

in the theoretical model. The presence of higher order modes is unlikely, as highly accurate frequency measurements in these bands revealed no significant radiated power.

VII. EXPERIMENTAL STUDIES OF CYCLOTRON EFFECTS IN OVERMODED BWO'S

To study the effects of finite magnetic fields, the cathode accelerating potential and the beam current were held constant to within ±10% and the axial magnetic field strength was varied between 2.6 kG $\leq B_z \leq 13.5$ kG. The magnetic field measurement accuracy was better than ±2%. The experiments were conducted with overmoded ($D/\lambda \sim 3$), sinusoidally corrugated SWS with lengths of 10- and 14-periods. Table III summarizes the beam and magnetic field parameters for the experiments.

At $B_z = 10$ kG, the radiated power still exhibits a dependence on the magnetic field strength. Not surprisingly, there is better agreement between the measured data and the finite magnetic field model than with the infinite magnetic field model. While there is still a discrepancy between the calculated and measured peak efficiencies, there is generally excellent agreement between the measured and calculated frequencies. The quality of this agreement is a strong indication that a pure $TM_{01}^{\odot}$ mode was produced by the 10- and 14-period overmoded structures.

A. Measurements of Radiated Microwave Power

Fig. 21(a) and (b) plots the radiated RF power as a function of axial magnetic field strength for the 10- and 14-period structures, respectively. Both plots exhibit a local power minimum at $B_z \simeq 6$ kG. Such dips in power as a function of magnetic field have been widely reported in nonovermoded BWO's [14], [15] and have been attributed to the absorption (reradiation) of the RF wave in the SWS into a cyclotron wave on the electron beam.

B. Comparison of Experimental Results with Nonlinear Theory

To study the effect of finite magnetic fields, the nonlinear theory described in Section VI-D was extended to include full three-dimensional relativistic motion of the beam electrons and to account for beam coupling to cyclotron waves [16]. As before, the model uses a slowly varying envelope function to approximate the electromagnetic fields in the structure and treats the specific case of BWO operation near cutoff by modeling the lowest order symmetric cold-structure dispersion curve as a parabolic function in k. The formulism allows the beam electrons to simultaneously interact with both forward

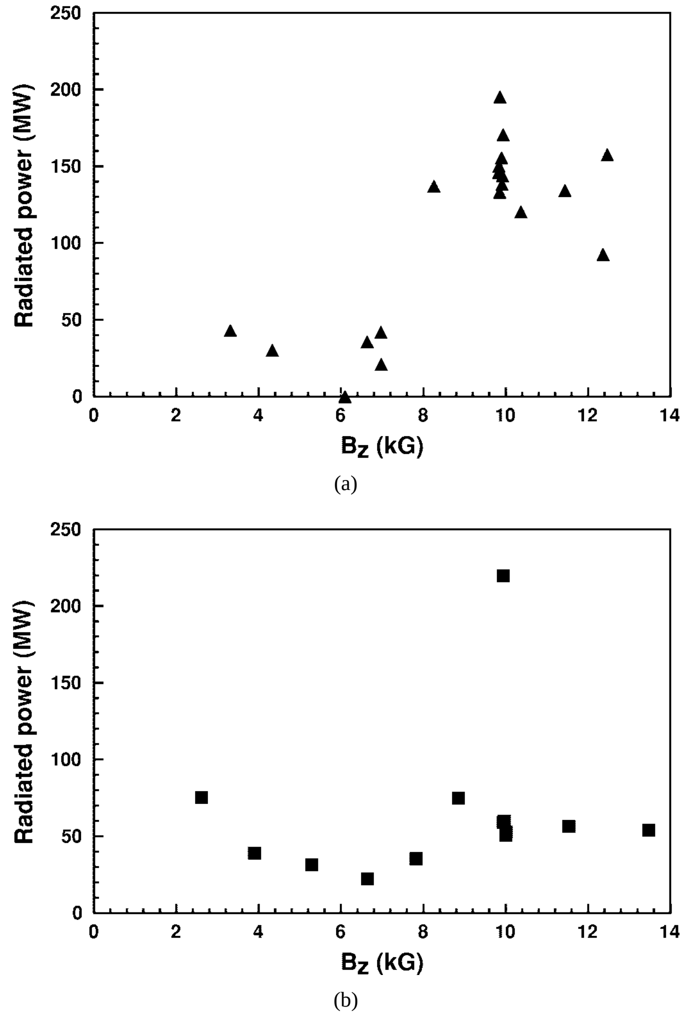

Fig. 21. BWO radiated RF power versus B_z with ϕ_c and I_b held constant to within $\pm 10\%$ for (a) 10-period and (b) 14-period structures.

and backward waves at a specified frequency, a particularly important feature as it is when both the forward and backward waves satisfy the cyclotron resonance condition that RF absorption by the beam overcomes the emission and the characteristic (B_z dependent) dips in BWO efficiency are observed.

Fig. 22(a) and (b) plots the experimentally measured frequency versus axial magnetic field along with computations made with nonlinear BWO model. The model used scaled versions of experimental voltage and current waveforms as input with peak voltages and currents as summarized in Table III. As was seen in the case of the infinite magnetic field model, the agreement between theory and experiment improves with increasing structure length. However, even in the case of the shorter (ten-period) structure, there is excellent agreement between the model and the experimental data; as seen in Fig. 22(a), the model and data agree to within better than 4% of each other.

Fig. 23(a) and (b) shows the corresponding plots of experimental and theoretical peak BWO efficiency as a function of axial magnetic field. As seen in Section VI-D, there is a large discrepancy in the magnitudes of experimental and theoretical plots, but the general shape of the two curves tracks well.

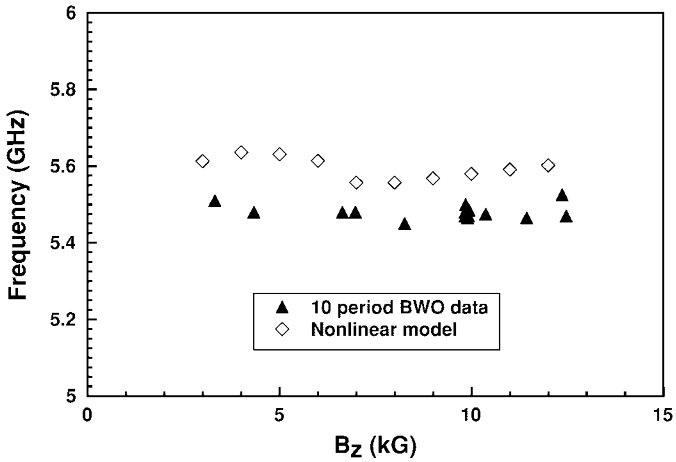

(a)

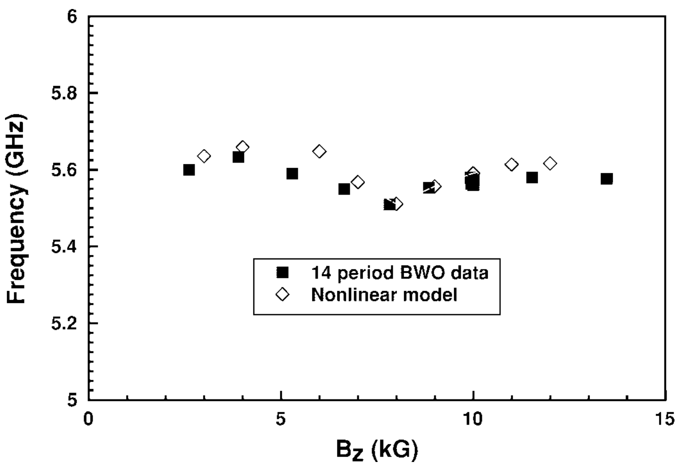

(b)

Fig. 22. BWO interaction frequencies versus B_z. Beam voltages and currents were held constant to within $\pm 10\%$. (a) Ten-period structure with $\phi_c = 571$ kV and $I_b 6.9$ kA (nominal) and (b) 14-period structure with $\phi_c = 550$ kV and $I_b = 7.2$ kA (nominal).

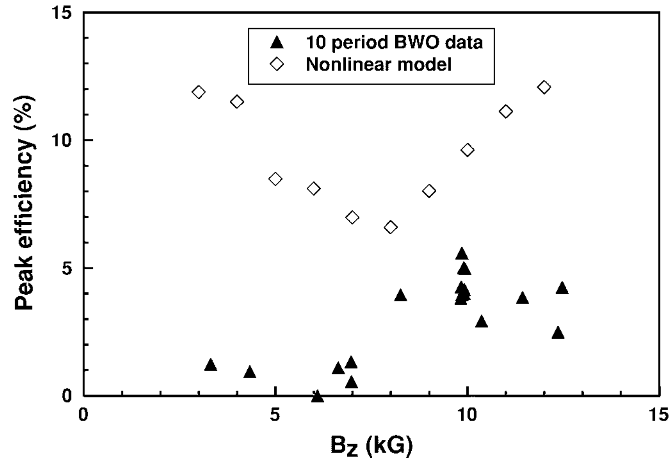

(a)

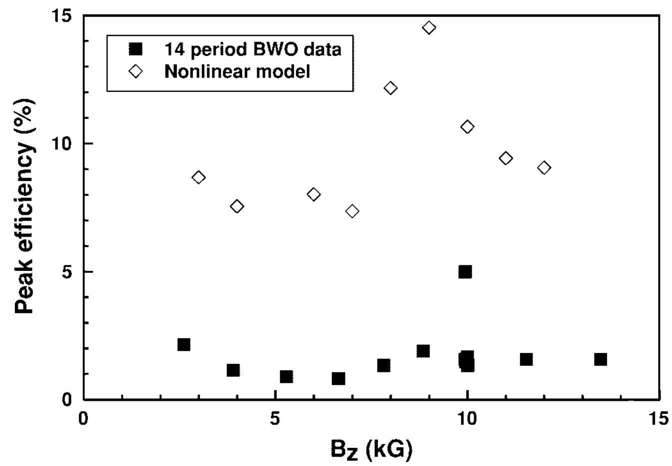

(b)

Fig. 23. BWO peak efficiencies versus B_z. Beam voltages and currents were held constant to within $\pm 10\%$. (a) Ten-period structure with $\phi_c = 571$ kV and $I_b = 6.9$ kA (nominal) and (b) 14-period structure with $\phi_c = 550$ kV and $I_b = 7.2$ kA (nominal).

VIII. CONCLUSIONS

An overmoded $(D/\lambda \sim 3)$ sinusoidally corrugated SWS was designed for high-power operation between 5 and 6 GHz with some simplifying design approximations. Modular sinusoidal rings were fabricated so that the effect of varying the length of the electrodynamic structure could be studied experimentally. Microwave radiation generated in the BWO was guided down a 29.2-cm-diameter overmoded waveguide $(D/\lambda \sim 5)$ and radiated into a large anechoic chamber from a 1-m-diameter cylindrical-horn antenna.

A series of experiments with 10-, 14-, and 35-period electrodynamic structures produced high-power highly coherent radiation in the frequency range between 5.2 and 5.7 GHz. The spectral purity of the radiation was typically $\Delta f/f < 0.5\%$. The highest radiated power was obtained with a ten-period structure, which reproducibly generated ~200 MW of RF power.

The experimental data and subsequent analyses with recently developed nonlinear models strongly support the hypothesis that pure $TM_{01}^{\odot}$ mode radiation was generated with overmoded $(D/\lambda \sim 3)$ SWS. Although the measured radiation pattern was asymmetric and uncharacteristic of $TM_{01}^{\odot}$ mode radiation, the asymmetries can be traced to passive (spatial) mode conversion at waveguide interfaces, as documented by low-power system calibration tests. All other evidence—high-spectral purity, lack of measurable power at frequencies higher than the fundamental interaction frequency, wave polarization, and the generally good agreement with theory—indicates that a pure symmetric mode was generated.

The results of the experiments and modeling demonstrate that overmoded electrodynamic structures can be used to decrease internal electric field stresses while maintaining good spectral purity and avoiding multimode generation. The application of such structures can lead to increased output power and longer pulse durations from high-power microwave devices.

APPENDIX

Internal reflections in the overmoded waveguide and at the horn and radome were measured and minimized. Transmission and reflection measurements made with a $TM_{01}^{\odot}$-mode launcher and a network analyzer indicated strong reflections

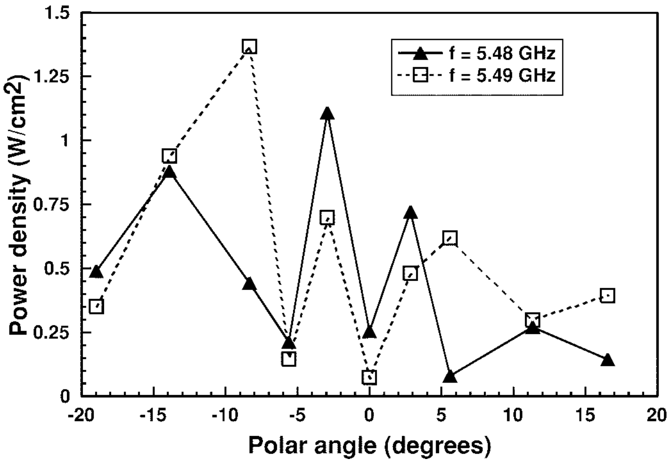

Fig. 24. Measured radiated power density pattern from a 250-kW pulsed-magnetron source, $f = 5.54$ GHz.

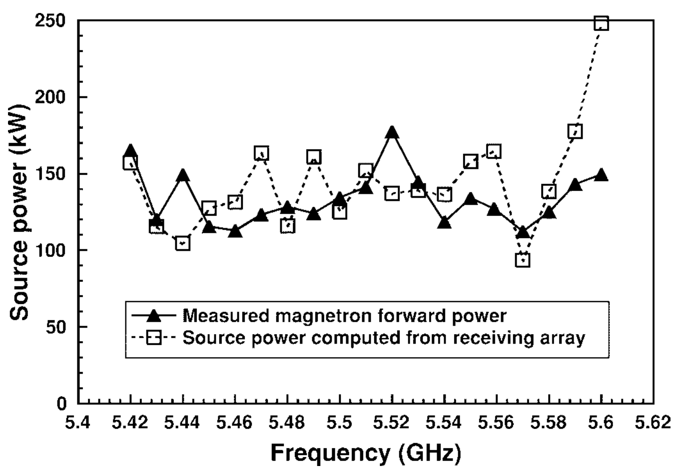

Fig. 25. Measured pulsed-magnetron source power compared with the source power computed from the monopole receiving array versus frequency.

at the joints in the vacuum waveguide sections. Sharp discontinuities at these joints were smoothed with copper tape, which largely eliminated the reflections from the edges. Over the frequency range of the experiment, the ratio of the reflected power to transmitted power was approximately -18 dB. The final vacuum joint, which was inaccessible and could not be smoothed with copper tape, and the hemispherical radome, which was constructed from an ~2-mm-thick fiberglass-epoxy composite, were the major sources of reflection in the system.

To provide an accurate measure of the microwave radiation pattern and generated power, the waveguide transmission system, output horn and radome, and monopole array were calibrated as a unit in their beam-driven experimental configuration. Referring to Fig. 9, the magnetized microwave interaction region was replaced by a 250-kW pulsed-magnetron source and a $TM_{01}^{\odot}$-mode launcher, which launched a pure TM_{01} circular-mode wave through the system; the resulting pattern in the anechoic chamber was measured with the monopole array. Ideally, the observed pattern should have exhibited rotational symmetry with a null on axis. However, asymmetric patterns were observed indicating that mode conversion had taken place (see, for example, Fig. 24). Spatial mode conversion in the waveguide transmission system and/or in the output antenna is the most likely cause of the observed asymmetries.

Despite the pattern asymmetries, we developed a pattern-integration technique that yielded reasonably good agreement with the measured magnetron source power. Estimates of total radiated microwave power were obtained from the asymmetric 1-D patterns by separately integrating the positive and negative polar angle portions of the radiation pattern (assuming symmetry in each case) and averaging the results. Source power estimates made in this manner were generally within about ± 1 dB of the measured magnetron source power over the frequency range 5.45–5.59 GHz (see Fig. 25). This technique was used to estimate the radiated power in all the beam-driven microwave experiments.

ACKNOWLEDGMENT

The authors would like to thank J. M. Cameron, D. Cohen, R. del Rosario, K. Ebersole, J. Golden, C. Lazard, P. Lezcano, J. Pyle, and J. R. Rodgers for their contributions in assisting in the experimental design and measurements.

REFERENCES

[1] J. Benford and G. Benford, "Survey of pulse shortening in high-power microwave sources," *IEEE Trans. Plasma Sci.*, vol. 25, pp. 311–317, Apr. 1997.
[2] G. Grabowski, J. M. Gahl, and E. Schamiloglu, "Electron emission from slow-wave structure walls in a long-pulse, high-power backward wave oscillator," *IEEE Trans. Plasma Sci.*, vol. 25, pp. 335–341, Apr. 1997.
[3] S. P. Bugaev, V. A. Cherepenin, V. I. Kanavets, V. I. Koshelev, V. A. Popov, and A. N. Vlasov, "Investigation of a millimeter-wavelength-range relativistic diffraction generator," *IEEE Trans. Plasma Sci.*, vol. 18, pp. 518–524, June 1990.
[4] S. P. Bugaev, V. A. Cherepenin, V. I. Kanavets, A. I. Klimov, A. D. Kopenkin, V. I. Koshelev, V. A. Popov, and A. I. Slepkov, "Relavistic multiwave Čerenkov generators," *IEEE Trans. Plasma Sci.*, vol. 18, pp. 525–536, June 1990.
[5] A. F. Alexandrov, S. Yu. Galuzo, V. I. Kanavets, and V. A. Pletyushkin, "Surface wave excitation by electron flow in a diaphragmatic waveguide," *Sov. J. Tech. Phys.*, vol. 51, pp. 1727–1730, 1981.
[6] J. A. Swegle, J. W. Poukey, and G. T. Leifeste, "Backward-wave oscillators with rippled wall resonators: Analytic theory and numerical simulation," *Phys. Fluids*, vol. 28, no. 9, pp. 2882–2894, Sept. 1985.
[7] J. A. Swegle, "Analytic theory of the backward-wave oscillator: Dispersion characteristics," Sandia Nat. Lab., SAND84-1796, 1984.
[8] B. N. Brejzman and D. D. Ryutov, "Powerful relativistic electron beams in a plasma and in a vacuum (theory)," *Nucl. Fusion*, vol. 14, pp. 879–907, 1974.
[9] A. Bromborsky and B. Ruth, "Calculation of TM_{0n} dispersion relations in a corrugated cylindrical waveguide," *IEEE Trans. Microwave Theory Tech.*, vol. MTT-32, pp. 600–605, June 1984.
[10] B. T. Smith, *Matrix Eigensystem Routines—EISPACK Guide*, 2nd ed. New York: Springer-Verlag, 1976.
[11] G. J. Rohwein, "Description and operating instructions: TEMPO high voltage microwave driver," Sandia Nat. Lab., Sandia Rep. SAND87-0851, 1988.
[12] S. M. Miller, T. M. Antonsen, Jr., B. Levush, A. Bromborsky, D. K. Abe, and Y. Carmel, "Theory of relativistic backward wave oscillators operating near cutoff," *Phys. Plasmas*, vol. 1, no. 3, pp. 730–740, Mar. 1994.
[13] B. Levush, T. M. Antonsen, Jr., A. Bromborsky, W-R Lou, and Y. Carmel, "Theory of relativistic backward-wave oscillators with end reflections," *IEEE Trans. Plasma Sci.*, vol. 20, pp. 263–280, June 1992.
[14] Y. Carmel, J. Ivers, R. E. Kribel, and J. Nation, "Intense coherent Čerenkov radiation due to the interaction of a relativistic beam with a slow-wave structure," *Phys. Rev. Lett.*, vol. 33, pp. 1278–1282, 1974.
[15] Yu. F Bondar, S. I. Zavorotnyi, A. L. Ipatov, N. I. Karbushev, N. F. Kovalev, O. T. Loza, G. P. Mkheidze, A. A. Ovchinnikov, A. A. Rukhadze, and L. E. Tsopp, "Measurements of RF emission from a carcinotron with a relativistic electron beam," *Sov. J. Plasma Phys.*, vol. 9, no. 2, pp. 223–226, Mar./Apr. 1983.

[16] S. M. Miller, T. M Antonsen, Jr., B. Levush, and A. N. Vlasov, "Cyclotron resonances in relativistic BWO's operating near cutoff," *IEEE Trans. Plasma Sci.*, vol. 24, pp. 859–869, June 1996.

David K. Abe (M'92) was born in Queens, NY, in 1959. He received the B.Sc. degree (engineering, with honors) from Harvey Mudd College, Claremont, CA, the M.Sc. (EE) degree from the University of California, Davis, and the Ph.D. degree from the University of Maryland, College Park, in 1981, 1988, and 1992, respectively.

From 1982 to 1988, he was with the Lawrence Livermore National Laboratory, Livermore, CA, where he supported the nuclear design program. From 1992 to 1994 he was employed as a Research Scientist with Berkeley Research Associates, Springfield, VA, where he worked on pulsed-power and high-power microwave projects. He joined the Army Research Laboratory in 1994, where he pursued projects in electromagnetic effects and high-power microwave generation. In 1997, he joined the Vacuum Electronics Branch of the Naval Research Laboratory, Washington, DC, where he is currently pursuing research projects in the areas of linear beam, slow-wave microwave devices, and materials.

Dr. Abe was awarded a Thomas J. Watson Foundation Fellowship in 1981 to study traditional music in Ireland.

Yuval Carmel (S'66–M'69–SM'90) was born in Israel in 1942. He received the B.Sc. and M.Sc. degrees from the Technion, Israel Institute of Technology, Haifa, Israel, in 1966 and 1971, respectively, and the Ph.D. degree from Cornell University, Ithaca, NY, in 1974, all in electrical engineering.

He was with the Israeli government for 15 years, the Naval Research Laboratory, Washington, DC, from 1981 to 1983, and has been with the University of Maryland, College Park, since 1988. His research interests include electromagnetic radiation from intense electrons beams, plasma microwave devices, advanced concepts in millimeter-wave tubes, gyrotrons, and backward-wave oscillators.

Susanne M. Miller (S'87–M'88) received the B.S., M.S. (both in electrical engineering), and Ph.D. degrees from the University of Maryland, College Park, in 1988, 1990, and 1995, respectively.

Her background in electrical engineering includes work in electrophysics, microelectronics, and digital signal processing with an emphasis on developing computer models for predicting microwave device performance. In 1996, she joined the Advanced Projects and Applications Division at ENSCO, Inc., Springfield, VA where she is primarily involved in developing signal processing algorithms for the characterization of underground facilities in support of the DoD Counter Proliferation Initiative. Her current interests are in the areas of predictive modeling of electromagnetic, seismic and acoustic signatures and the application of short-pulse electromagnetics for imaging buried objects.

Alan Bromborsky was born in Irvington, NJ, in 1946. He received the B.S.E.E degree (with honors) from the Newark College of Engineering (now the New Jersey Institute of Technology), NJ, in 1968, and the M.S. degree in physics from the University of Chicago, IL, in 1973.

In 1969, he joined the U.S. Army Harry Diamond Laboratories (now part of the Army Research Laboratory). From 1969 to 1976 his work area included nuclear weapons effects (IEMP and weapons effects simulation with electron and ion beams). Since 1977 he has concentrated on the effects of high-power microwaves and the development of microwave sources from modest to ultra-high power levels (experiments on FX-45, TEMPO, and Aurora intense relativistic electron-beam generators). His current interest includes developing tools (parametric models and codes) for the optimization of high-power (10^4–10^6 W) high-perveance broad-band microwave amplifiers.

Baruch Levush (M'88–SM'90), for a biography, see this issue, p. 415.

Thomas M. Antonsen, Jr. (M'87), for a biography, see this issue, p. 425.

William W. Destler (M'84–SM'90–F'92) received the B.S. degree from the Stevens Institute of Technology, Hoboken, NJ, in 1968 and the Ph.D. degree from Cornell University, Ithaca, NY, in 1972.

He is presently Dean of Engineering at the University of Maryland at College Park. He is the author or co-author of over 100 research papers on these and related topics. His research interests have been primarily in the areas of high-power microwave engineering sources and advanced accelerator technology.

Dr. Destler is the recipient of numerous awards for teaching excellence, including the 1989 AT&T/ASEE Award for Excellence in Engineering Education for the Mid-Atlantic States. He is a Fellow of the American Physical Society.